Viscoelasticity and shear flow of concentrated, noncrystallizing colloidal suspensions: Comparison with mode-coupling theory

Miriam Siebenbürger

Physikalische Chemie I, University of Bayreuth, 95440 Bayreuth, Germany

Matthias Fuchs

Fachbereich Physik, Universität Konstanz, 78457 Konstanz, Germany

Henning Winter

Chemical Engineering Department, University of Massachusetts, Amherst Box 33110, Amherst, MA 01003-3110

Matthias Ballauff[a]

Physikalische Chemie I, University of Bayreuth, 95440 Bayreuth, Germany

Synopsis

We present a comprehensive rheological study of a suspension of thermosensitive particles dispersed in water. The volume fraction of these particles can be adjusted by the temperature of the system in a continuous fashion. Due to the finite polydispersity of the particles (standard deviation: 17%), crystallization is suppressed and no fluid-crystal transition intervenes. Hence, the moduli G' and G'' in the linear viscoelastic regime as well as the flow curves (shear stress $\sigma(\dot{\gamma})$ as function of the shear rate $\dot{\gamma}$) could be measured in the fluid region up to the vicinity of the glass transition. Moreover, flow curves could be obtained over a range of shear rates of 8 orders of magnitude, while G' and G'' could be measured spanning over 9 orders of magnitude. Special emphasis has been laid on precise measurements down to the smallest shear rates/frequencies. It is demonstrated that mode-coupling theory generalized in the integration through transients framework provides a full description of the flow curves as well as the viscoelastic behavior of concentrated suspensions with a single set of well-defined parameters.
© 2009 The Society of Rheology. [DOI: 10.1122/1.3093088]

I. INTRODUCTION

The flow behavior of concentrated suspensions of hard sphere particles in a shear flow is a long-standing problem in colloid physics [Russel *et al.* (1989); Larson (1999)]. The most prominent feature of these systems is the strong increase in the zero-shear viscosity
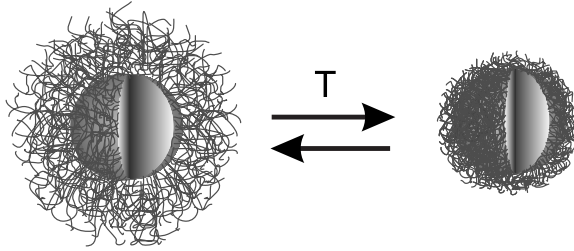
---

[a]Author to whom correspondence should be addressed; electronic mail: matthias.ballauff@uni-bayreuth.de

with increasing volume fraction ϕ. Concomitantly, there is a strong increase in the storage modulus G'. Moreover, with increasing shear rate a marked shear thinning sets in where the relative viscosity η/η_S (η_S: viscosity of solvent) is lowered considerably. These general features are also observed for solutions of soft colloidal particles as, e.g., a solution of star polymers in a suitable solvent [Helgeson *et al.* (2007)]. Suspensions of hard spheres or of particles characterized by a sufficiently steep mutual repulsion may hence be treated as the most simple model system for the rheological study of the flow behavior of colloidal systems, including of colloidal glasses [Petekidis *et al.* (2002); Pham *et al.* (2008)].

By now, it is recognized that many aspects of the dynamics of quiescent suspensions of hard spheres can be understood and modeled quantitatively in terms of the mode-coupling theory (MCT) [van Megen and Pusey (1991); van Megen and Underwood (1994)]. MCT [Götze and Sjögren (1992)] was shown to explain quantitatively the (near complete) structural arrest that takes place in colloidal dispersions above the volume fraction $\phi_g \approx 0.58$ for almost monodisperse hard spheres. Moreover, this value of ϕ_g has turned out to be quite compatible with experimental studies of the zero-shear viscosity η_0 [Meeker *et al.* (1997); Cheng *et al.* (2002)]. Here it has been demonstrated that the strong upturn of η_0 occurs much below the volume fraction of 0.63 that would refer to the random close packing of the spheres. First theoretical calculations of η_0 within the frame of MCT fully supported this view [Banchio *et al.* (1999)].

Fuchs and Cates (2002, 2003) recently demonstrated that MCT can be generalized to treat the dynamics of colloidal suspension in shear flow. They developed the integrations through transients (ITT) approach, which describes the competition between enforced deformation or flow and intrinsic structural relaxation. Thus, MCT can be used to model the distortion of the structure of suspensions by a flow field at finite shear rate $\dot{\gamma}$. One central point of this theory is the melting of the glass by shear. Flow leads to a glass-to-fluid transition in the suspension and a unique stationary state can be reached again despite the fact that the volume fractions of the particles in the suspension are above ϕ_g. It is presumed that this holds as long as local "free volume" is available below the random close packing. Flow curves giving the relative viscosity η/η_S as function of shear rate are predicted to present well-defined states that are independent of the previous history of the sample. In addition to these predictions from ITT-MCT pertaining to the nonlinear flow of suspensions, MCT is capable of describing the linear viscoelastic behavior of concentrated dispersions. In this way, MCT offers a complete modeling of the rheological properties of dispersions at high packing fractions ϕ or for strong particle interactions close to vitrification, in the absence of shear ordering, shear banding, and shear thickening, which are neglected. First comparisons with simulations indeed demonstrated that the theory captures the salient features of the flow behavior of flowing suspensions for small enough shear rates [Varnik and Henrich (2006)].

Recently, it has been demonstrated that suspensions of thermosensitive particles present excellent model systems studying the flow of concentrated suspensions for a quantitative comparison of the theory of Fuchs and Cates to experimental data [Fuchs and Ballauff (2005); Crassous *et al.* (2006a, 2008a)]. The particles consist of a solid core of polystyrene onto which a thermosensitive network of poly(N-isopropylacrylamide) (PNIPAM) is attached ([Crassous *et al.* (2006b, 2008b)], see Fig. 1). The PNIPAM shell of these particles swells when immersed in cold water (below 32 °C). Water gets expelled at higher temperatures leading to a considerable shrinking. Thus, for a given number density, the effective volume fraction ϕ_{eff} can be adjusted within wide limits by adjusting the temperature. Senff *et al.* (1999) were the first to demonstrate the use of these particles as a model system for studying the dynamics in concentrated suspensions

FIG. 1. Schematic representation of the thermosensitive core-shell particles used in this study. The polymer chains are affixed to the surface of the core. Immersed in cold water, the thermosensitive network will swell. The degree of swelling can be reduced by raising the temperature. At 32 °C, a volume transition takes place in which most of the water is expelled from the network.

[Senff *et al.* (1999)]. Similar microgel particles have been used to study the dynamics of concentrated suspensions and the aging in these systems [Purnomo *et al.* (2006, 2007)]. The advantages of these systems over the classical hard sphere systems are obvious. Dense suspensions can be generated *in situ* without shear and mechanical deformation. Moreover, all previous history of the sample can be erased by raising the temperature and thus lowering the volume fraction to the fluid regime. Hence, subtle effects as, e.g., aging can be studied by these systems in a nearly ideal fashion [Purnomo *et al.* (2006, 2007)]. Moreover, microgels can be used as models for pastes and gels in which the effective volume fraction of the particles exceeds unity by far [Seth *et al.* (2006)].

Previous investigations using dispersions of thermosensitive core-shell particles have demonstrated that MCT is indeed able to model the flow curves as well as the linear viscoelasticity of concentrated suspensions [Crassous *et al.* (2006a, 2008a)]. In particular, this theory allows us to calculate G' and G'' as function of the frequency ω from data that have been obtained from the analysis of flow curves [Crassous *et al.* (2008a)]. However, a problem that restricted this comparison was crystallization due to the narrow size distribution of the particles. Crystallization presents a major obstacle since the rate of nucleation is rather fast for volume fractions even far below the volume fraction ϕ_g of the glass transition ($\phi_g \approx 0.58$). The crystalline phase could be removed by shear melting and the fluid state could be supercooled for a given time. The time window of nucleation, however, limited the experimental studies to frequencies and/or shear rates not too small [Crassous *et al.* (2006a, 2008a)]. A fully conclusive comparison of MCT with experimental data, however, requires that measurements extend down to the smallest frequencies and shear rates [Fuchs and Ballauff (2005); Crassous *et al.* (2008a)].

Here we present a full comparison of theory and experiment using a thermosensitive suspension having a slightly broader size distribution that prevents crystallization. Hence, all measurements can now be extended to very low shear rates or frequencies that may take hours without any disturbance by crystallization. It will be demonstrated that MCT provides indeed a full description of the rheological behavior of suspension under homogeneous flow, except for a glassy relaxation process presently not understood. While we find no indications of shear banding [Callaghan (2008); Dhont and Briels (2008); Manneville (2008); Olmsted (2008)] and other effects that may come into play for concentrated suspensions [Isa *et al.* (2007)], we cannot fully exclude these effects in our study. Yet, they would presumably destroy the tight connection between quiescent and shear-driven dynamics which we find.

The paper is organized as follows. In Sec. II we give a brief survey of the main predictions of MCT. In particular, the equations in a schematic model of MCT used for

the evaluation of data as well as the fit parameters necessary for a comparison with experimental data are discussed. For an extensive description of MCT, the reader is deferred to a recent paper [Crassous *et al.* (2008a)]. After a section devoted to the description of the systems and the measurements, a comprehensive comparison of MCT with flow curves as well as with linear viscoelastic properties will be given. A major focus is the low frequency and long time behavior which had not been accessible before. Special attention will be paid to the fact that MCT is capable of describing both the flow curves as well as G' and G'' as functions of frequency. A brief Conclusion will sum up the main findings. An Appendix summarizes for completeness the microscopic ITT-MCT equations and describes a second fit performed to the linear response moduli.

II. MCT OF FLOWING SUSPENSIONS: MAIN PREDICTIONS

The central points and main predictions of MCT and its generalization to flowing dispersions in the ITT approach were recently discussed in detail [Crassous *et al.* (2008a)]. Hence, it will suffice to discuss the points that will be used in the analysis of the experiments. Structural relaxation, which is the central topic of MCT, leads to internal relaxation processes with an intrinsic relaxation time τ that far exceeds the dilute limit Brownian diffusion time. The ITT-MCT approach to sheared fluids considers the effect of shear when the dressed Peclet or Weissenberg number $Pe = \dot{\gamma}\tau$ becomes appreciable, while the bare Peclet number $Pe_0 = 6\pi\eta_s R_H^3 \dot{\gamma}/(k_B T)$ formed with the solvent viscosity η_s and the hydrodynamic particle radius R_H should be much lower than unity for the approach to hold.

The main point of the MCT of quiescent dispersions is the slowing down of the dynamics at the glass transition. Critical values for the particle concentration, the temperature, or other thermodynamic control variables exist, where a glass transition separates fluid from yielding glassy states. In fluid states, a first Newtonian region is reached if the shear rate or the frequency is low enough; the Newtonian viscosity $\eta_0 = \eta(\dot{\gamma}\to 0)$ is finite. Non-Newtonian flow, that is, shear thinning, is observed at higher shear rates corresponding to a finite Weissenberg number $Pe \approx 1$. MCT recovers Maxwell's relation $\eta_0 \propto \tau$, so that the criterion $Pe \approx 1$ translates into $\eta_0 \dot{\gamma} \approx G_\infty^c$, where $G_\infty^c = G'(\omega \to 0)$ is the (zero frequency) shear modulus at the glass transition. For glassy states at higher densities or interaction parameters, Newtonian flow is not observed anymore but the shear stress σ is predicted to approach a plateau value for sufficiently low shear rates $\dot{\gamma}$; a dynamic yield stress follows $\sigma^+ = \sigma(\dot{\gamma}\to 0) > 0$. It corresponds to an infinite Newtonian viscosity.

A central point of MCT as applied to flowing suspensions [Fuchs and Cates (2002)] is shear melting. Finite shear rates will lead to a melting of the glass into a fluid. As a consequence of this, flow curves given by the shear stress σ as function of the shear rate $\dot{\gamma}$ present well-defined states for a given volume fraction even above the glass transition. Hence, $\sigma(\dot{\gamma})$ is independent of the previous history of the sample, under the condition that the stationary long time limit has been achieved. Previous experimental studies strongly suggested that this central prediction of theory is found indeed [Crassous *et al.* (2006a, 2008a)]. However, in all previous experiments, crystallization intervened at sufficiently low shear rates and this point is in need of further experimental elucidation.

In the following, the main equations used for the evaluation of the rheology data within a schematic model of MCT are briefly summed up. The Appendix describes the (more fundamental) microscopic equations. Within the *schematic* $F_{12}^{(\dot{\gamma})}$ model [Fuchs and Cates (2003)] Brownian motion of the particles is captured in terms of a density correlator $\Phi(t)$, which is normalized/initiated according to $\Phi(t \to 0) = 1 - \Gamma t$. MCT relates this

correlation function to the memory function $m(t)$ by a memory equation,

$$\partial_t \Phi(t) + \Gamma \left\{ \Phi(t) + \int_0^t dt' m(t-t') \partial_{t'} \Phi(t') \right\} = 0. \tag{1}$$

The parameter Γ describes the microscopic dynamics of the density correlator and will depend on structural and *hydrodynamic* correlations. The memory function describes stress fluctuations which become slower when approaching the volume fraction of the glass transition. In the $F_{12}^{(\dot\gamma)}$ model, the memory function is written as

$$m(t) = \frac{v_1 \Phi(t) + v_2 \Phi^2(t)}{1 + (\dot\gamma t / \gamma_c)^2}. \tag{2}$$

This model, for the quiescent case $\dot\gamma = 0$, was suggested by Götze in 1984 [Götze (1984, 1991)] and describes the development of slow structural relaxation upon approaching a glass transition; actually, there is a line of glass transitions in the model, which are reached by increasing the coupling vertices/parameters v_1 and v_2 to their critical values $v_1^c = (2\lambda - 1)/\lambda^2$ and $v_2^c = 1/\lambda^2$, where the so-called exponent parameter λ with $1/2 \leq \lambda \leq 1$ parametrizes the (type-B) glass transition line. Under shear, an explicit time dependence of the couplings in $m(t)$ captures the accelerated loss of memory by shear advection [Fuchs and Cates (2002, 2003, 2008)]. Shearing causes the dynamics to decay for long times because fluctuations are advected to smaller wavelengths, where small scale Brownian motion relaxes them. The parameter γ_c sets the scale for the accumulated strain $\dot\gamma t$ to matter.

Equations (1) and (2) will be used with the choice of vertices $v_2 = v_2^c = 2$ (corresponding to $\lambda = 1/\sqrt{2}$) and $v_1 = v_1^c + \varepsilon(1 - f^c)/f^c$, where $v_1^c = 0.828$. The critical glass form factor f^c, which takes the value $f^c = (1 - \lambda) = 0.293$ for this choice, describes the frozen-in structure obtained from $\Phi(t \to \infty, \varepsilon = 0, \dot\gamma = 0) = f^c$ at the glass transition in the absence of shear. The glass transition lies at $\varepsilon = 0$, where the Newtonian viscosity diverges. Under shear, glass states are molten, but the transition still separates shear thinning fluid states $\varepsilon < 0$, where a Newtonian viscosity exists, from yielding glassy states $\varepsilon \geq 0$, where a dynamic yield stress σ^+ exists. The specific choice of this transition point is motivated by (i) its repeated use in the literature and (ii) because it predicts a divergence of the viscosity at the glass transition with a power law exponent γ close to the one of the microscopic MCT calculation for short ranged repulsions,

$$\eta_0 \propto \tau \propto (-\varepsilon)^{-\gamma}, \quad \text{with} \quad \gamma = \gamma(\lambda = 1/\sqrt{2}) = 2.34.$$

Within microscopic MCT for hard spheres using the Percus-Yevick structure factor, $\gamma = 2.46$ was found [Götze and Sjögren (1992)].

The correlator $\Phi(t)$ obtained by numerical solution of Eq. (1) may then be used to calculate the generalized shear modulus $g(t, \dot\gamma)$ according to

$$g(t, \dot\gamma) = v_\sigma \Phi^2(t) + \eta_\infty \delta(t - 0+), \tag{3}$$

where v_σ is a parameter measuring the strength of stress fluctuations; the quadratic expression is motivated by the microscopic MCT summarized in the Appendix. The parameter η_∞ models the short time high-frequency viscosity that characterizes viscous processes which require no structural relaxation. Together with Γ, it is the only model parameter affected by solvent mediated interactions. Steady state shear stress under constant shearing and viscosity then follows via integrating up the generalized modulus,

$$\sigma = \eta\dot{\gamma} = \dot{\gamma}\int_0^\infty dt g(t,\dot{\gamma}) = \dot{\gamma}\int_0^\infty dt v_\sigma \Phi^2(t) + \dot{\gamma}\eta_\infty. \tag{4}$$

When setting the shear rate $\dot{\gamma}=0$ in Eq. (2) so that the schematic correlator belongs to the quiescent equilibrium system, the frequency dependent moduli of the linear response framework follow from Fourier transforming:

$$G'(\omega) + iG''(\omega) = i\omega\int_0^\infty dt e^{-i\omega t}g(t,\dot{\gamma}=0) = i\omega\int_0^\infty dt e^{-i\omega t}v_\sigma\Phi^2(t)_{\dot{\gamma}=0} + i\omega\eta_\infty. \tag{5}$$

Because of the vanishing of the Fourier integral in Eq. (5) for high frequencies, the parameter η_∞ can be directly identified as high-frequency viscosity,

$$\lim_{\omega\to\infty} G''(\omega)/\omega = \eta_\infty^\omega, \quad \text{with} \quad \eta_\infty^\omega = \eta_\infty. \tag{6}$$

At high shear, on the other hand, Eq. (2) leads to a vanishing of $m(t)$ and Eq. (1) gives an exponential decay of the transient correlator $\Phi(t) \to e^{-\Gamma t}$ for $\dot{\gamma}\to\infty$. The high-shear viscosity thus becomes

$$\eta_\infty^{\dot{\gamma}} = \lim_{\dot{\gamma}\to\infty} \sigma(\dot{\gamma})/\dot{\gamma} = \eta_\infty + \frac{v_\sigma}{2\Gamma} = \eta_\infty^\omega + \frac{v_\sigma}{2\Gamma}. \tag{7}$$
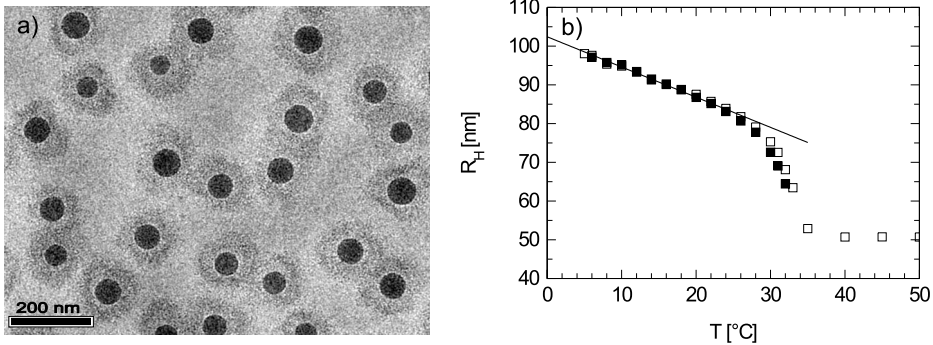
Equation (7) connects the high-shear viscosity with the high-frequency limit of the viscosity in an analytical manner. Moreover, both $\eta_\infty^{\dot{\gamma}}$ and η_∞^ω are accessible from experimental data and Eq. (7) provides an additional check for internal consistency of the fit within the frame of the schematic model. Representative solutions of the $F_{12}^{(\dot{\gamma})}$ model have been discussed recently [Crassous *et al.* (2008a); Fuchs and Cates (2003); Hajnal and Fuchs (2008)].

III. EXPERIMENTAL

The particles consist of a solid core of poly(styrene) onto which a network of crosslinked PNIPAM is affixed [Crassous *et al.* (2006b, 2008b)]. The degree of crosslinking of the PNIPAM shell effected by the crosslinker N,N′-methylenebisacrylamide (BIS) was 2.5 mol %. The core-shell type PS-PNIPAM particles were synthesized, purified, and characterized as described by Dingenouts *et al.* (1998). Immersed in water, the shell of these particles is swollen at low temperatures. Raising the temperature above 32 °C leads to a volume transition within the shell. Cryogenic transmission electron microscopy (cryo-TEM) and dynamic light scattering (DLS) were used to investigate the structure and swelling of the particles [Crassous *et al.* (2006b, 2008b)]. Further experimental details on cryo-TEM are given by Crassous *et al.* (2006b).

The average size and size distribution of the particles were determined with the CPS Disk Centrifuge from LOT, model DC 24000 at 24 000 rpm in an aqueous glucose density gradient between 3 and 7 wt % as medium at room temperature. The number-average diameter determined at 25 °C is 131 nm and the standard deviation of the size distribution is 17%.

DLS was done with a Peters ALV 800 light scattering goniometer. The temperature was controlled with an accuracy of 0.1 °C. In the range of temperatures used for the measurements, R_H could be linearly extrapolated between 6 °C and 25 °C ($R_H = -0.7796\cdot T + 102.4096$ with T as the temperature in °C) as it was done in Crassous *et al.* (2006a). Figure 2(b) displays R_H as the function of temperature. Moreover, this plot

FIG. 2. (a) Cryo-TEM micrograph of the core-shell particles in water. The core-shell structure (black core, gray shell) can be seen clearly. (b) Results of the DLS measurements of the latex at various temperatures. Closed squares represent the hydrodynamic radius measured in aqueous 0.05 mol L^{-1} KCl; open squares measurements in pure water. All rheological experiments presented here have been done using particles dissolved in aqueous 0.05 mol L^{-1} KCl solution [Crassous *et al.* (2006a, 2008a)]. In this way, possible electrostatic interaction between the particles due to the residual charges affixed to the core particles can be screened totally. Below the volume transition, the decrease in the hydrodynamic radius R_H is linear in very good approximation ($R_H = -0.779\ 6 \cdot T + 102.409\ 6$ with T being the temperature in °C; see solid line in graph).

demonstrates that R_H can be obtained very precisely. Since the subsequent reduction in the data (see below) involves a scaling of the data by R_H^3, this fact is of great importance.

Density measurements have been made using a DMA-60 densiometer supplied by Paar (Graz, Austria). The density for the core-shell particles was determined as follows: $\varrho = 1.118$ g cm^{-3} at 25 °C, 1.124 g cm^{-3} at 20 °C, 1.125 g cm^{-3}, at 18 °C, and 1.126 g cm^{-3} at 17 °C. These densities can be described with the function $\varrho = 6.800 \times 10^{-7} \cdot T^3 + 1.129$ with the temperature T in °C. In all experiments reported herein, 5 $\times 10^{-2}$ mol L^{-1} KCl were added to the suspensions in order to screen the remaining electrostatic interactions caused by a few charges attached to the surface of the core particles. Previous studies have shown that this screening is fully sufficient. Thus, within the range of volume fractions under consideration here, the thermosensitive particles can be regarded as hard spheres [see the discussion of this point in Crassous *et al.* (2006a)].

The flow behavior and the linear viscoelastic properties for the range of the low frequencies were measured with a stress-controlled rotational rheometer Physica MCR 301 (Anton Paar) equipped with a Couette system (cup diameter: 28.929 mm; bob diameter: 26.673 mm; and bob length: 39.997 mm). For comparison, the double gap geometry (inner cup diameter: 23.820 mm; inner bob diameter: 24.660 mm; outer bob diameter: 26.668 mm; outer cup diameter: 27.590 mm; and bob length: 40.00 mm) was used as well. Measurements have been performed on 12 mL (Couette single gap geometry) and 4 mL (Couette double gap geometry) solution and the temperature was set with an accuracy of ±0.05 °C. Deformation tests were done from a deformation of 0.1 to 100% in the case of the dynamic deformation test with a logarithmic time ramp of 200 to 20 s at 1 Hz. The shear stress σ versus the shear rate $\dot{\gamma}$ (flow curve) was measured after a preshearing of $\dot{\gamma} = 100$ s^{-1} for 2 min and a waiting time of 10 s. The flow curves were obtained setting $\dot{\gamma}$ to a given value; first with increasing $\dot{\gamma}$ from $\dot{\gamma} = 10^{-5} - 10^3$ s^{-1} with a logarithmic time ramp from 1500 to 20 s. Then after a waiting time of 10 s $\dot{\gamma}$ was decreased again. The frequency dependence of the loss G'' and elastic G' moduli has been measured after a 2 min preshear at a shear rate of 100 s^{-1} and 10 s waiting time for 1% strain from 10 to 10^{-4} Hz with a logarithmic time ramp from 20 to 600 s. The dependence upon the strain has been checked and confirmed that all the measurements were performed in the linear

regime. In order to limit solvent evaporation during the long measurement runs, a coverage of a metal cap (available with the rheometer), a layer of parafilm® (from Pechiney plastic packaging) for sealing the gaps of the metal cap, a layer of humid tissues, and again a layer of parafilm® was used. The solid content was determined before and after the experiment by weighting the sample before and after drying. So, the concentration of the solution in the experiment was determined to 8.90 wt % ± 0.1 wt %. G' and G'' at elevated frequencies were obtained using the piezoelectric vibrator (PAV) [Crassous *et al.* (2005)] and cylindrical torsional resonator (TR) [Deike *et al.* (2001); Fritz *et al.* (2003)] supplied by the Institut für dynamische Materialprüfung, Ulm, Germany. The PAV was operated from 10 to 3000 Hz. The solution is placed between two thick stainless steel plates. One remains static, whereas the second is cemented to piezoelectric elements. The gap was adjusted with a 50 μm ring. A set of piezoelectric elements is driven by an ac voltage to induce the squeezing of the material between the two plates. The second set gives the output voltage. Experimental details concerning this instrument are given elsewhere [Crassous *et al.* (2005)]. The cylindrical TR used was operated at a single frequency (26 kHz). The experimental procedure and the evaluation of data were described recently [Deike *et al.* (2001); Fritz *et al.* (2003)].

IV. RESULTS AND DISCUSSION

A. Characterization

Recent work showed that cryo-TEM is an excellent tool for the analysis of the core-shell particles used for the present study [Crassous *et al.* (2006b, 2008b)] because this method allows us to visualize the particles *in situ*, that is, directly in the aqueous suspension. Figure 2 displays a micrograph of the suspension obtained by cryo-TEM. The core-shell structure of the particles is clearly visible as already demonstrated by previous work [Crassous *et al.* (2006b, 2008b)]. Since the polydispersity of the present suspension is considerably higher than the dispersion used in our previous study [Crassous *et al.* (2008a)], the system does not crystallize anymore even if kept for a prolonged time at volume fractions above 50%. However, Fig. 2 demonstrates that the suspension used here is still a well-defined model system. Hence, it can be used for a comprehensive comparison of experimental data with MCT. Attempts to suppress crystallization by mixing core-shell particles of slightly different size failed to produce reliable results, since crystallization in these systems was found to be only slowed down but not suppressed totally.

While the aspect that the higher polydispersity of the suspension used here suppresses crystallization is essential for studying the glass transition, this prevents the precise determination of the effective volume fraction ϕ_{eff} using the density at which crystallization occurs [Cheng *et al.* (2002)]. This convenient and precise procedure was used in our previous study on a narrowly distributed thermosensitive system [Crassous *et al.* (2006a, 2008a)]. In this way, the zero-shear viscosity as well as the high-frequency and the high-shear viscosities could be obtained as functions of ϕ_{eff}. The effective volume fraction ϕ_{eff} in a polydisperse solution may in principle be determined from the mass balance as outlined in previous studies [Crassous *et al.* (2006a, 2008a)]. However, the error in this determination turned out to be of appreciable magnitude. The effective volume fraction ϕ_{eff} could also not be calculated as for monodisperse particles by precise measurements of the hydrodynamic radius R_H, the core radius, and the mass ratio of core and shell as done by Crassous *et al.* (2008a). Unfortunately, polydispersity leads to an error which is too large and no meaningful data could be obtained. Furthermore, viscosity measurements in the dilute state and the use of the Batchelor-Einstein equation for the relative zero-shear viscosity could not be applied because of the appreciable polydisper-
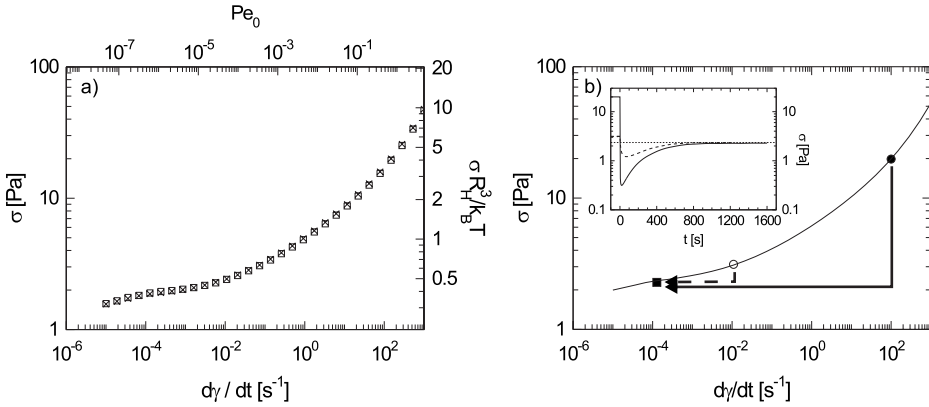
sity, too. In lack of other convincing procedures, we follow the procedure suggested by Cheng *et al.* (2002) who observed that the high-frequency viscosity is relatively insensitive to polydispersity. Thus the effective volume fraction is obtained by comparing the relative viscosities at infinite frequency with the monodisperse core-shell system used by Crassous *et al.* (2008a). This will be discussed in further detail in conjunction with Fig. 6 below.

B. Reversibility of flow curves

A central prediction of MCT is the full reversibility of the flow curves, that is, of the shear stress σ as function of the shear rate $\dot{\gamma}$. This is evident for any volume fraction below the volume fraction ϕ_g of the glass transition. Here the system is ergodic and a well-defined steady state must be reached for sufficiently long time. This point is well borne out by all experiments done so far [Crassous *et al.* (2006a, 2008a)]. However, a totally different situation arises above ϕ_g. In the glassy state, the suspension becomes nonergodic and the flow curves may become ill defined. Hence, for concentrated suspensions of large non-Brownian particles dispersed in a highly viscous medium, the measured shear stress is found to be dependent on the previous history of the sample [Heymann and Aksel (2007)]. MCT, however, predicts that shear melting sets in at any finite shear rate $\dot{\gamma}$. Therefore, shear flow restores the ergodicity in the system and the thermal motion of the spheres can erase all traces of the previous deformations of the sample if flow is applied over a sufficiently long time interval. Two types of experiments need to be done to explore these basic principles in further detail. (i) Each data point giving $\sigma(\dot{\gamma})$ must be independent regardless of the shear history. Thus, flow curves $\sigma(\dot{\gamma})$ should be fully reversible regardless whether the data are taken by increasing rate or decreasing the shear rate. The reversibility of the flow curves has already been demonstrated in previous work. However, the suspensions analyzed previously [Crassous *et al.* (2006a, 2008a)] began to crystallize during the long measurements needed for exploring the dynamics at smallest shear rates $\dot{\gamma}$. To overcome this problem, the present system is sufficiently polydisperse, so that crystallization is suppressed. Figure 3 displays the resulting flow curves down to $Pe_0 = 10^{-6}$. The onset of a plateau is clearly seen. Additional experiments with long waiting times demonstrated that crystallization does not occur in the present system. Moreover, Fig. 3(a) points to another important fact: $\sigma(\dot{\gamma})$ is entirely independent of the geometry of the rheometer used for studying the flow behavior. Figure 3(a) demonstrates this fact by overlaying the resulting $\sigma(\dot{\gamma})$ obtained from single gap and double gap Couette geometry. If shear banding would play any role [Callaghan (2008); Dhont and Briels (2008); Manneville (2008); Olmsted (2008)], the resulting $\sigma(\dot{\gamma})$ should be different and depend definitely on the width of the gap of the instrument. The difference in the curvature for the two experiment geometries would have resulted in different onsets of shear banding. Also, shear banding in the double gap Couette system would have resulted in a complex interplay of instabilities in the two gaps. None of this is observed here.
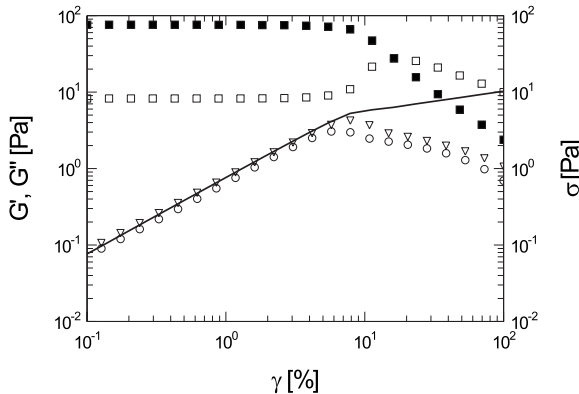
(ii) The full reversibility of the flow curves are demonstrated also by a second type of experiment [Fig. 3(b)]. Here a stationary state is first obtained for a given shear rate $\dot{\gamma}$. Then a much lower shear rate is adjusted and the resulting shear stress is monitored as a function of time. Figure 3(b) shows that $\sigma(\dot{\gamma})$ converges to the stationary value measured previously [solid line in Fig. 3(b)]. The inset displays the evolution of $\sigma(\dot{\gamma})$ with time. Evidently, a long time may be needed until the stationary value is reached. However, all data demonstrate that the full reversibility of $\sigma(\dot{\gamma})$ is fully supported by our experiment also above the glass transition. One of the central predictions is thus fully corroborated.

FIG. 3. (a) Reversibility of the flow curves for a 7.87 wt % suspension at 12 °C with two different geometries: Couette single gap geometry (crosses) and double gap geometry (squares). (b) Reversibility of the flow curves by comparing jump experiments and the flow curve (solid line) measured from higher to lower shear rates at 8.42 wt % and 14.75 °C. The steady state shear stress values of jumps from different shear rates to one as shown by the arrows in the graph are plotted for two examples: jump from 100 s^{-1} (full circle) to 0.000127 s^{-1} (full square) and jump from 0.0108 s^{-1} (hollow circle) to 0.000127 s^{-1} (full square). (b) Inset: the same jumps are plotted time dependent. The different jumps are plotted as follows: jump from 100 s^{-1} to 0.000127 s^{-1} (thick solid line) and jump from $0.010\,8$ s^{-1} to $0.000\,127$ s^{-1} (thick dashed line). The thin short dashed line in the inset represents the shear stress value at $0.000\,127$ s^{-1} of the flow curve for the same concentration and temperature.

Deviations observed previously [Crassous *et al.* (2008a)] were solely due to the crystallization of the sample which is suppressed in the present system. In this way, flow curves may to a certain extent be compared to thermodynamic results; they are fully independent of the path leading to a given state.

A point to be considered further is the transition from the linear to the nonlinear viscoelastic regime in the glassy regime. Figure 4 displays G', G'', as well as σ for different deformations at a rate of 1 Hz. The data show that the linear regime is preserved up to a strain of nearly 10%. The same finding was also seen by Petekidis *et al.* (2002) and by Le Grand and Petekidis (2008) for a comparable system. Moreover, $G'\gamma$ measured

FIG. 4. Comparison of the dynamic strain sweep at 1 Hz (G': filled squares; G'': open squares; and σ: solid line) and a continuous strain sweep with two different measurement times for each point (20 s per point: triangles down and 200 s per point: circles) for a 8.90 wt % suspension at 17 °C ($\phi_{\text{eff}} = 0.641$).

for different strains γ coincides directly with the measured stress σ. Hence, within this range of γ, the glassy suspension behaves as a homogeneous solid as expected. Again, shear banding or possible inhomogeneities within the gap should disturb this type of measurement. Figure 4 demonstrates that this is not seen. Obviously, these experiments are not fully sufficient to rule out shear banding entirely. However, the good agreement between two entirely different types of experiments with theory to be discussed further below points clearly to the fact that shear banding does not disturb the measurements reported here.
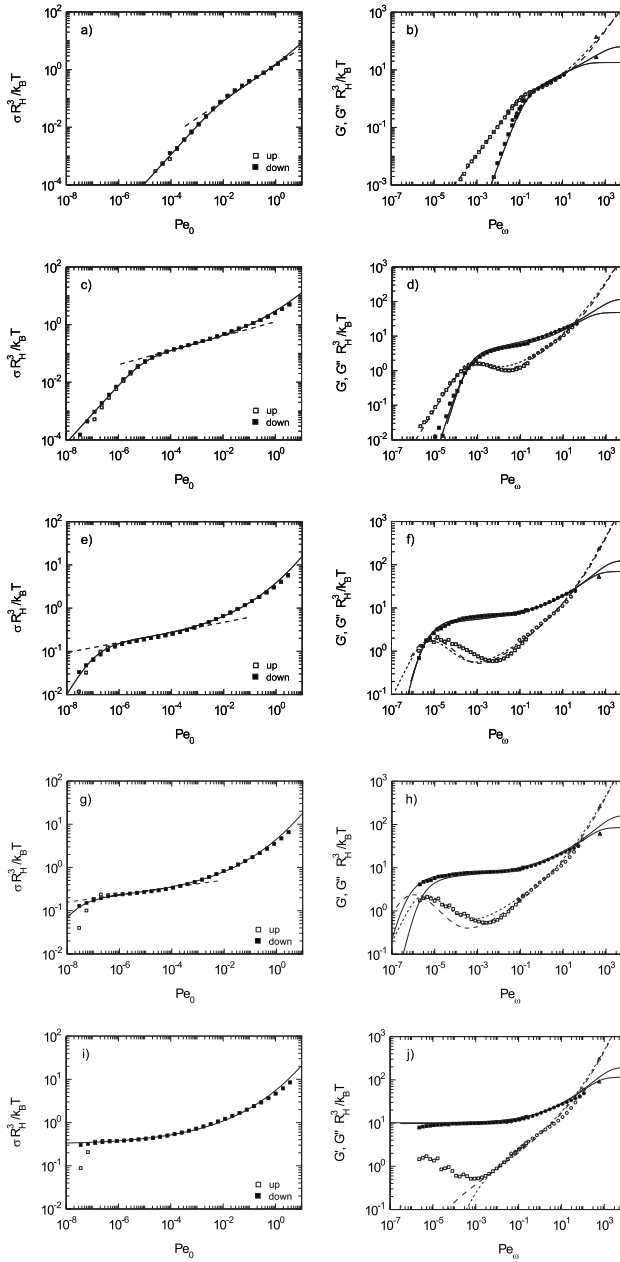
Beyond a strain of ca. 10%, the shear melting of the glass starts and the measured stress σ is considerably lower than the value calculated from G'. Figure 4 indicates that the linear viscoelastic regime is extended over a sufficiently large range of deformations.

C. Comparison with mode-coupling theory: Schematic model

A thorough comparison of ITT-MCT to experimental data must be related not only to the flow curves discussed in Sec. IV B but also to the data obtained for the linear viscoelasticity, that is, for G' and G'' as functions of the frequency ω. A previous comparison [Crassous *et al.* (2008a)] demonstrated that both sets of data can indeed be described by a generalized modulus $g(t, \dot{\gamma})$ as introduced in Sec. II. However, at smallest Pe_0 crystallization intervened and the comparison was restricted to intermediate to high-shear rates/frequencies. Crystallization is suppressed for the present system and a fully quantitative comparison of theory and experiment now becomes possible down to $Pe_0 \approx 10^{-8}$ in case of the flow curves. G' and G'' can be obtained down to $Pe_\omega \approx 10^{-6}$. Here, the frequency dependent Peclet (or Deborah) number defined as $Pe_\omega = 6\pi \eta_s R_H^3 \omega / (k_B T)$ compares the frequency with the time it takes a particle to diffuse its radius R_H at infinite dilution. At high densities, structural relaxation shows up at $Pe_\omega \ll 1$.

In the following, we shall compare the experimental flow curves and G' and G'' with theory for a given effective volume fraction ϕ_{eff}. Figure 5 gives this comparison for five different effective volume fractions. On the left-hand side, the flow curves $\sigma(\dot{\gamma})$ are presented as functions of the bare Peclet number Pe_0; on the right-hand side G' and G'' are displayed as the functions of Pe_ω, now calculated with the respective frequencies ω. Open and closed symbols used in the flow curve plots indicate stresses measured during increasing (up) or decreasing (down) the shear rate, respectively. Some small degree of hysteresis is seen only at the highest densities, where the exceedingly slow intrinsic dynamics prevents (presumably) the up states to have reached stationarity, while the higher shear during the history of the down states (presumably) has melted any long lived contributions. As ITT-MCT considers the stationary state, only the flow curve data during decreasing the shear rate ("down") are addressed in the following. The up data are shown to assess the hysteresis. Table I gathers the respective volume fractions of the samples studied in Fig. 5 together with the other experimental conditions. Note that G' and G'' have been obtained over nearly 7 orders of magnitude in frequency by combining a Couette rheometer with the PAV and the TR.

The generalized shear modulus $g(t, \dot{\gamma})$ [cf. Eq. (3)] presents the central theoretical quantity used in this fit. Within the schematic model, the vertex prefactor v_σ is kept as a shear-independent quantity. It can easily be obtained from the stress and modulus magnitudes. Hydrodynamic interactions enter through η_∞, which can be obtained from measurements done at high frequencies, and through Γ, which can be obtained via Eq. (7) from measurements done at high-shear rates. Given these three parameters, both the shapes of the flow curves as well as the shapes of the moduli G' and G'' may be obtained as functions of the two parameters ε and $\dot{\gamma}/\gamma_c$. The former sets the separation to the glass

FIG. 5. Left column: reduced flow curves for different volume fractions (graphs in left column *a*, *c*, *e*, *g*, and *i*). Open squares represent the "'up'" curve from low to high-shear rates; closed squares represent the "'down" curve from high to low shear rates. The solid lines are the results of the schematic model; the dashed line represents the pseudopower law behavior (see Table II). Right column: reduced frequency dependent moduli for different volume fractions (graphs *b*, *d*, *f*, *h*, and *j* in right column). Full symbols/solid lines represent G'; hollow symbols/dashed lines represent G''. Squares mark the data points obtained by the Physica MCR 301; circles with the PAV; triangles up with the TR; the thick lines are the results of the schematic model; and the thin lines are the results of the microscopic model. Graphs in one row represent the continuous and dynamic measurements at one volume fraction. *a* and *b* were measured at 8.90 wt % and 25 °C with $\phi_{\text{eff}} = 0.519$; *c* and *d* were measured at 7.87 wt % and 18 °C with $\phi_{\text{eff}} = 0.600$; *e* and *f* at 8.90 wt % and 20 °C with $\phi_{\text{eff}} = 0.626$; *g* and *h* at 8.90 wt % and 19 °C with $\phi_{\text{eff}} = 0.639$; and *i* and *j* at 8.90 wt % and 17 °C with $\phi_{\text{eff}} = 0.641$.

TABLE I. Experimental parameters (concentration c, temperature T, and calculated ϕ_{eff}) of the measurements shown in Fig. 5. The fit parameter v_σ, Γ, γ_c, and η_∞ of the F_{12}^γ model as well as the calculated values $\eta_\infty^{\dot\gamma}$, σ_0, and η_0 are written in terms of the respective normalization.

c (wt %)	T (°C)	ϕ_{eff}	ε	v_σ $\left[\frac{k_BT}{R_H^3}\right]$	Γ $\left[\frac{D_0}{R_H^2}\right]$	γ_c	$\eta_\infty = \eta_\infty^\omega$ $\left[\frac{k_BT}{D_0R_H}\right]$	$\eta_\infty^{\dot\gamma}$ [a] $\left[\frac{k_BT}{D_0R_H}\right]$	σ_0 [b] $\left[\frac{k_BT}{R_H^3}\right]$	η_0 [c] $\left[\frac{k_BT}{D_0R_H}\right]$
8.90	25	0.519	-0.072000	18	20	0.0845	0.2250	0.6750		1.1345×10^1
7.87	18	0.600	-0.003500	48	50	0.1195	0.2400	0.7200		7.7439×10^3
8.90	20	0.626	-0.000420	70	80	0.1414	0.3938	0.8313		1.0177×10^6
8.90	19	0.639	-0.000170	85	90	0.1491	0.4250	0.8972		9.1562×10^6
8.90	17	0.641	0.000021	115	120	0.1622	0.4313	0.9104	3.3193×10^{-1}	

[a]Calculated by Eq. (7).
[b]Extrapolated from the fits using the $F_{12}^{(\dot\gamma)}$ model.
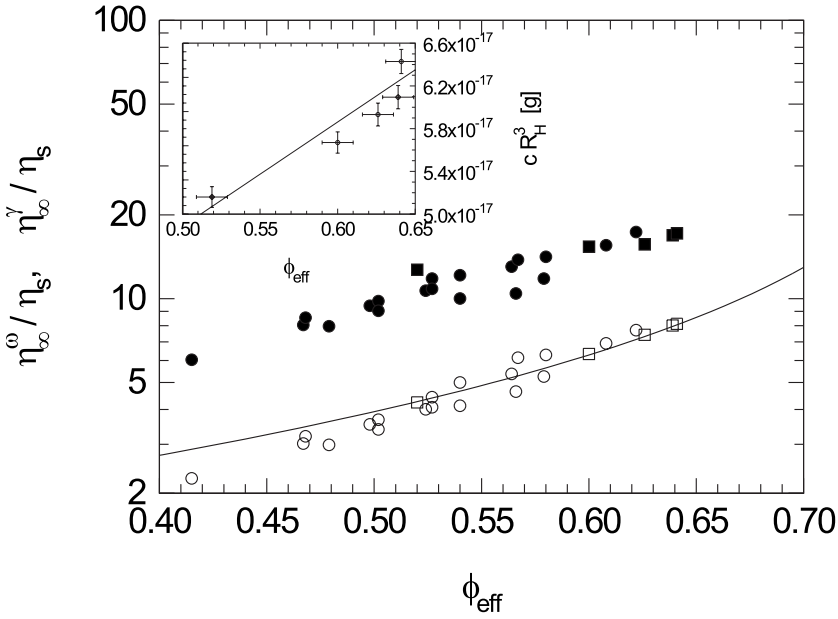[c]Directly measured for the three lower volume fractions extrapolated for the two highest volume fraction from the fits using the $F_{12}^{(\dot\gamma)}$ model.

transition and thus (especially) the longest relaxation time, while the latter tunes the effect of the shear flow on the flow curve. The characteristic changes in the shapes of the steady stress and the moduli are dominated by ε and $\dot\gamma/\gamma_c$.

The fitting of the data was done as follows. All measured quantities, namely, σ, G', and G'', were converted to the respective dimensionless quantities by multiplication with R_H^3/k_BT where R_H is the hydrodynamic radius at the respective temperature. Previous work has demonstrated that the effective volume fraction deriving from R_H is the only decisive thermodynamic parameter [Crassous *et al.* (2006a, 2008a)]. As already discussed above, $\dot\gamma$ and ω are converted by $6\pi\eta_s R_H^3/k_BT$ to the respective Peclet numbers.

Evidently, both reduced moduli, the Pe numbers, and the packing fraction depend on the effective particle volume R_H^3. Therefore, this quantity must be measured with utmost precision. In our polydisperse sample, actually a distribution of values R_H^3 exists, whose variance we determined by disk centrifugation at low concentration. It is important to note that the size distribution is set when filling the sample and changes only smoothly with temperature during the measurements reported in Fig. 5. Because we study a small region in packing fractions close to the glass transition, we may assume the size distribution to be (almost) constant. Therefore, we have $R_H^3(T)$ (the third moment of the size distribution) as a single experimental control parameter, whose small change upon varying temperature T drives the system through the glass transition (see also the discussion in Fig. 6).

Subsequently, the fit procedure is started at the smallest volume fraction and a trial value for the separation parameter ε is chosen. This fit can be done very accurately since the resulting reduced moduli depend very sensitively on ε. Once the overall shape of both the reduced stress $\sigma R_H^3/k_BT$ and of the reduced storage and loss modulus has been reproduced by a proper choice of ε, the vertex parameter v_σ is obtained. For lower volume fraction, the crossing point of G' and G'' may be used; near the glassy state the plateau value of σ and G' can be used. Note that in all steps, both sets of data, that is, the flow curves as well as G' and G'', must be fitted with the same v_σ. Next Γ is determined from the dynamic data which are fully described with this choice of parameters. Given Γ, the parameter γ_c [see Eq. (2)] is chosen so that the experimental flow curves are matched by theory. Then η_0, σ_0, and $\eta_\infty^{\dot\gamma}$ can be calculated. The results of these fits are gathered in Table I. We reiterate that the final set of parameters must lead to a description of both the flow curves as well as of the dynamic data. This requirement stresses the connection of

FIG. 6. Estimation of the effective volume fractions ϕ_{eff} for the polydisperse system used here. The relative high-frequency viscosities obtained for a monodisperse latex (hollow circles; [Crassous *et al.* (2008a)]) are plotted against the effective volume fraction. These high-frequency viscosity η_∞^ω can be fitted by the Lionberger-Russel equation [see Eq. 4.22 in Lionberger and Russel (1994)] by assuming partial draining of the network of the shell [Deike *et al.* (2001)]. Assuming the same relation for the polydisperse latex under consideration here, η_∞^ω was used to determine the effective volume fractions (see hollow squares). The ϕ_{eff} obtained by this way are plotted in the inset versus the concentration c $[g \cdot m \ L^{-1}]$ times the cubed hydrodynamic radius R_H^3 $[m^3]$. The solid line in the inset represents the linear scaling of an effective volume fraction and $c \cdot R_H^3$ with a slope of 9.67×10^{-17} g and an intercept of zero. As a further check, the high-shear viscosities (filled symbols) are plotted as well as a function of ϕ_{eff}. The closed circles show this quantity for the narrowly distributed latex [Crassous *et al.* (2008a)], whereas the closed squares denote the respective quantities for the present system used the effective volume fraction thus derived. Good agreement is seen thus corroborating the present way of estimating ϕ_{eff}.

the equilibrium structural relaxation at the glass transition to the nonlinear rheology under strong flow, which is one of the central points of the ITT-MCT approach.

Figure 5 demonstrates that the rheological behavior of a noncrystallizing colloidal dispersion can be modeled in a highly satisfactory manner by five parameters that display only a weak dependence on the effective volume fraction of the particles. Increasing the effective packing fraction drives the system toward the glass transition, viz., ε increases with ϕ_{eff}. Stress magnitudes (measured by v_σ) also increase with ϕ_{eff}, as do high-frequency and high-shear viscosities; their difference determines Γ. The strain scale γ_c remains around the reasonable value of 10%. In spite of the smooth and small changes in the model parameters, the F_{12}^γ model achieves to capture the qualitative change in the linear and nonlinear rheology. The measured Newtonian viscosity increases by a factor around 10^5. The elastic modulus G' at low frequencies is utterly negligible at low densities, while it takes a rather constant value around $10k_BT/R_H^3$ at high densities. An analogous observation holds for the steady state shear stress $\sigma(\dot{\gamma})$, which at high densities takes values around $0.3k_BT/R_H^3$ when measured at lowest shear rates. For lower densities, shear rates larger by a factor around 10^7 would be required to obtain such high stress values.

At volume fractions around 0.5, the suspension is Newtonian at small Pe_0 (see Fig. 5).

Clearly, these flow curves are fully reversible since the suspension is still in the fluid regime. The schematic model provides a perfect fit. Moreover, the theory demonstrates in full agreement with experiment that the high-shear viscosities measured in shear flow and the high-frequency viscosities measured in the linear viscoelastic regime do not agree, as had already been known from simulations and experiments [Foss and Brady (2000); Russel *et al.* (1989); Phan *et al.* (1999); Horn *et al.* (2000)]. As is evident from Eq. (7), both $\eta_\infty^{\dot\gamma}$ and η_∞^ω are related by Eq. (7) and the Cox-Merz rule does not hold for suspensions as expected. Approaching the glass transition leads to a characteristic S-shape of the flow curves and the Newtonian region becomes more and more restricted to the region of smallest Pe_0. Concomitantly, a pronounced minimum in G'' starts to develop, separating the slow structural relaxation process from faster, rather density independent motions; while G' exhibits a more and more pronounced plateau. At the highest densities (panels i and j in Fig. 5), the theory would conclude that a yielding glass is formed, which exhibits a finite elastic shear modulus (elastic constant) $G_\infty = G'(\omega \to 0)$ and a finite dynamic yield stress $\sigma^+ = \sigma(\dot\gamma \to 0)$. The experiment shows, however, that small deviations from this glasslike response exist at very small frequencies and strain rates. These deviations and the clear difference in G'' at low frequencies indicate that the used idealized version of ITT-MCT, which contains the prediction of an ideal quiescent glass (nonergodic state), fails at $\phi_{\mathrm{eff}} = 0.641$. Some decay mechanism of this state different from the shear induced melting exists, which is not captured by the theory. It presumably develops smoothly and is already present at lower densities shown in panels g and h, where it explains the (small) quantitative deviations. Description of this ultraslow process requires extensions of the present ITT-MCT [Crassous *et al.* (2008a)], where additional physical mechanisms for stress relaxation need to be considered that are neglected here. The present analysis, however, leads to an estimate of the glass transition density ϕ_g around 0.640, which will not (appreciably) be shifted to higher values when the extended ITT-MCT model of Ref. Crassous *et al.* (2008a) is used. As carefully analyzed there for states deeper in the glass regime, the extended plateau region in the elastic modulus G' and in the flow curve rules out to interpret the state shown in panels g and h as fluid one in the ITT-MCT framework. We expect that extended data will firmly establish $\phi_{\mathrm{eff}} = 0.641$ as a nonideal glass state in the present system, which is fluidized by a transport mechanism of unknown origin and not contained in the present theory.

D. Power laws

Often power law shear thinning is discussed, when the viscosity is plotted as a function of shear rate instead of the flow curves, viz., stress versus shear rate. For fluid states, the double logarithmic presentation in Fig. 5 shows characteristically S-shaped flow curves, which have a point of inflection. Clearly, this flow curve being a more sensitive presentation as the usual $\eta(\dot\gamma)$ plots rules out the existence of a true power law behavior, which should show up as a straight line in the double logarithmic plot. Yet, at the point of inflection of the S-curve, and closely around it, a pseudopower law may exist. Here $\eta(\dot\gamma) \sim \dot\gamma^{(p-1)}$, where p is the slope of the tangent in the flow curve at the inflection point $p = d\ln\sigma / d\ln\dot\gamma$. These tangents are indicated by dashed straight lines in the panels of Fig. 5. The pseudopower law that corresponds to the one in the viscosity can describe the flow curve over more than two decades in shear rate. The exponents p (it is included in Table II) change with density and can be computed within the schematic model [Hajnal and Fuchs (2009)]. Nevertheless, Fig. 5 shows clearly that the description by power laws is by far inferior to the one provided by MCT.

TABLE II. Experimental parameters (concentration c, temperature T, and experimental effective volume fraction ϕ_{eff}. The parameters of the microscopic MCT calculations [separation parameter ε, volume fraction ϕ with $\phi_g = 0.5159$, c_y, and D_S/D_0, where $D_0 = k_B T/(6\pi\eta_s R_H)$], as shown in Fig. 5 are listed here. Furthermore, the power law exponents p from the dashed lines in the flow curves of Fig. 5 are given in this table.

c (wt %)	T (°C)	ϕ_{eff}	ε	ϕ	c_y	D_s/D_0	p
8.90	25	0.519	−0.10000	0.4643	2.3	0.3	0.631
7.87	18	0.600	−0.00794	0.5118	2.3	0.3	0.248
8.90	20	0.626	−0.00126	0.5153	2.3	0.3	0.117
8.90	19	0.639	−0.00100	0.5154	3.0	0.3	0.0852
8.90	17	0.641	0.00158	0.5167	3.5	0.3	

E. Effective volume fraction

As already outlined in Sec. III, the effective packing fraction ϕ_{eff} could not be determined by the convenient and accurate method to map to the value at freezing, as used previously. Hence, we followed the suggestion of Cheng *et al.* (2002) and compared the high-frequency viscosities of the narrowly distributed system studied previously [Crassous *et al.* (2008a)] with the respective values determined directly for the present system. We proceed as follows: The high-frequency viscosities η_∞^ω obtained previously for the similar but monodisperse system [Crassous *et al.* (2008a)] are plotted in Fig. 6 (hollow circles) against the volume fraction ϕ_{eff}, which could be determined precisely for this system. Following previous work [Deike *et al.* (2001)], a fit of these data by the respective expression developed by Lionberger and Russel (1994) can be achieved by assuming a partial draining of the network. Here we find that the effective radii thus obtained are smaller by ca. 8% than the values measured by DLS. The solid line in Fig. 6 displays this fit. The effective volume fractions of the present system have been obtained from this master curve (hollow squares in Fig. 6). The filled symbols in Fig. 6 display the high-shear viscosities obtained for the monodisperse system [filled circles; Crassous *et al.* (2008a)]. The respective values for the polydisperse system under scrutiny here are shown as filled squares in the same plot for the volume fractions thus obtained. Figure 6 demonstrates that both sets of data agree within the present limits of error. This shows that the present determination of ϕ_{eff} for the polydisperse system leads to reasonable estimates of this quantity. The values thus obtained are gathered in Table I. Moreover, the inset of Fig. 6 demonstrates that there is a linear relationship between the obtained ϕ_{eff} values and cR_H^3 as expected.

F. Microscopic MCT calculations

While schematic models provide a handy description of the universal features close to the glass transition and the shear melting of glasses, the microscopic formulation of ITT-MCT actually aims to predict from first principles the nonlinear rheology starting with the underlying particle interactions (see the Appendix for a short summary). Because of the anisotropy of the structure under shear, it has not been possible yet to solve the ITT-MCT equations without further approximations. Only solutions of schematic or isotropically averaged models are available under flow.

Yet, without shear the equations of quiescent MCT [Götze (1991)] can be solved readily and can be compared to the frequency dependent moduli within the linear response regime. This has been done considering the monodisperse system in Ref. Crassous *et al.* (2008a), and after determination of the effective packing fraction we could perform

identical calculations for the polydisperse system [see the Appendix and Ref. Crassous *et al.* (2008a) for details of the calculation which use the Percus-Yevick approximation to the structure factor of hard spheres]. Here, of course the simplification to do monodisperse MCT calculations to compare with the measurements in the polydisperse system adds to the errors in the comparisons. There are fewer adjustable parameters in the microscopic MCT calculation than in the schematic model calculation, namely, three. They are the effective collective short time diffusion coefficient, the effective packing fraction setting the separation to the glass transition, and a parameter c_y that corrects for the underestimate of the stress magnitudes by the microscopic MCT. All microscopic fit parameters are reported in Table II. Quite good agreement of the microscopic calculation for monodisperse hard spheres with the data can be achieved, with parameters that vary regularly with density and take quite reasonable values. Interestingly, the polydisperse system has larger moduli by a factor around 2 than the monodisperse system at the same effective packing fraction [compare with $c_y = 1.4$ in Ref. Crassous *et al.* (2008a)], and the separation parameter ε at the highest density takes a larger positive value in the fit using the microscopic MCT than in the fit using the schematic $F_{12}^{(\dot{\gamma})}$ model. Microscopic and schematic MCT fit to the linear moduli support each other well, putting the glass transition density in our polydisperse system to around $\phi_g = 0.640$. This value should not be brought into connection with ϕ_{rcp}: the value of random close packing of monodisperse hard spheres. It is well established that ϕ_{rcp} increases strongly with already modest polydispersity [Schaertl and Sillescu (1994)].

V. CONCLUSION

The fluid-to-glass transition in colloidal suspensions leads to characteristic changes in the flow curves and concomitantly of G' and G'' as the functions of frequency. Here we demonstrated that both sets of data can be quantitatively modeled by a single generalized modulus $g(t, \dot{\gamma})$. Moreover, $g(t, \dot{\gamma})$ can be fully described by MCT. Hydrodynamic interaction enters only through the high-shear and the high-frequency viscosities $\eta_\infty^{\dot{\gamma}}$ and η_∞^{ω}, respectively. MCT naturally includes that the latter quantities are not identical but closely related to each other [see the discussion in Eq. (7)]. Small deviations between data and theory are only seen for G'' in the immediate vicinity of the glass volume fraction and only at the lowest Peclet numbers Pe_ω. This finding can be assigned to a very slow relaxation that is not captured by MCT.

ACKNOWLEDGMENTS

APPENDIX

The ITT approach, which generalizes the MCT of the glass transition to colloidal dispersions under stationary shear [Fuchs and Cates (2002, 2008)], consists of equations of motion for a density correlator $\Phi_{\mathbf{q}}(t)$ which describes structural rearrangements and approximated Green-Kubo formulae relating stress relaxation to the decay of density fluctuations. The approach was described by Crassous *et al.* (2008a) and the used equations can be summarized as follows.

The density correlator obeys an equation of motion containing a retarded friction kernel which arises from the competition of particle caging and shear advection of fluctuations

$$\partial_t \Phi_{\mathbf{q}}(t) + \Gamma_{\mathbf{q}}(t) \left\{ \Phi_{\mathbf{q}}(t) + \int_0^t dt' m_{\mathbf{q}(t')}(t-t') \partial_{t'} \Phi_{\mathbf{q}}(t') \right\} = 0, \tag{8}$$

with the advected wave vector $\mathbf{q}(t)$, whose component along the gradient direction varies with time $q_y(t) = q_y(0) - \dot{\gamma} t q_x$ because of the affine component of the particle motion; while q_x and q_z remain time independent. The density correlator is normalized $\Phi_{\mathbf{q}}(t=0) = 1$. Its initial decay is described by $\Gamma_{\mathbf{q}}(t) = D_s q^2(t)/S_{q(t)}$, with D_s (or more precisely D_s/S_0) the collective short time diffusion coefficient, which may depend on hydrodynamic interactions, and thus differ from the Stokes-Einstein-Sutherland value. The equilibrium structure factor S_q encodes the particle interactions and introduces the experimental control parameters such as density and temperature. The generalized friction kernel $m_{\mathbf{q}'}(t)$, which is an autocorrelation function of fluctuating stresses, is approximated from the structural rearrangements captured in the density correlators,

$$m_{\mathbf{q}'}(t) = \frac{1}{2N} \sum_{\mathbf{k}} \frac{S_{q'(t)} S_k S_p}{q'^2(t) q'^2} V_{\mathbf{q}'\mathbf{k}\mathbf{p}}(t) V_{\mathbf{q}'\mathbf{k}\mathbf{p}}(0) \Phi_{\mathbf{k}}(t) \Phi_{\mathbf{p}}(t), \tag{9}$$

where the vertices are given by the equilibrium structure factor,

$$V_{\mathbf{q}\mathbf{k}\mathbf{p}}(t) = \mathbf{q}(t) \cdot (\mathbf{k}(t) n c_{k(t)} + \mathbf{p}(t) n c_{p(t)}) \delta_{\mathbf{q},\mathbf{k}+\mathbf{p}}, \tag{10}$$

with n the particle density, and c_k the Ornstein-Zernicke direct correlation function $c_k = (1 - 1/S_k)/n$. Similarly, the generalized shear modulus is approximated assuming that stress relaxations can be computed from integrating the transient density correlations,

$$g(t, \dot{\gamma}) = \frac{k_B T}{2} \int \frac{d^3 k}{(2\pi)^3} \frac{k_x^2 k_y k_y(-t)}{kk(-t)} \frac{S_k' S_{k(-t)}'}{S_k^2} \Phi_{\mathbf{k}(-t)}^2(t), \tag{11}$$

where $S_k' = \partial S_k/\partial k$.

The schematic $F_{12}^{(\dot{\gamma})}$ model described above follows from a simplification of these equations. It mimics using v_1 and v_2 the increase in the vertices $V_{\mathbf{q}\mathbf{k}\mathbf{p}}$ with sharpening structural correlations in S_q, which captures the cage effect causing a glass transition [Götze (1991); Götze and Sjögren (1992)]. It mimics with $1/(1 + (\dot{\gamma} t/\gamma_c)^2)$ the shear-driven decorrelation, which can be recognized from the vanishing of the memory kernel at long times under shear: $m_{\mathbf{q}'}(t\dot{\gamma} \gg 1) = 0$ and $m_{\mathbf{q}'}(t) - m_q(t)^{(\dot{\gamma}=0)} = \mathcal{O}((\dot{\gamma} t)^2)$ in the microscopic ITT equations [Fuchs and Cates (2002)]. Without shear $\dot{\gamma} \equiv 0$, Eqs. (8)–(11) become the familiar MCT equations which can readily be solved after discretization, as has been done in previous studies [Crassous *et al.* (2008a)]. The thin dashed lines in Fig. 5 labeled microscopic model result from these calculations, with parameters listed in Table II. But under shear, the equations become anisotropic and require more severe approximations, for example, using the simple schematic $F_{12}^{(\dot{\gamma})}$ model.

In detail, the microscopic MCT equations in the quiescent state were solved for a dispersion of monodisperse hard spheres with structure factor S_k taken from the Percus-Yevick approximation. The wave vector integrals in the microscopic model Eqs. (8)–(11) were discretized according to Ref. Crassous *et al.* (2008a) using $M = 600$ wave vectors chosen from $k_{\min} = 0.05/R_H$ up to $k_{\max} = 59.95/R_H$ with separation $\Delta k = 0.1/R_H$. Time was discretized with initial step width $dt = 2 \times 10^{-7} R_H^2/D_s$, which was doubled each time after 400 steps. Because the first principles calculations carry quantitative errors, which would

mask the qualitative comparison, two adjustments of parameters were performed for making the comparisons in Fig. 5. The magnitude of the linear modulus is too small in theory by a factor c_y which is included in Table II. The computed position of the glass transition is also somewhat too small; $\phi_g = 0.5159$ in MCT in monodisperse hard spheres relative to $\phi_g = 0.58$ for monodisperse, and $\phi_g = 0.640$ in the present polydisperse system studied in experiment. Therefore the relative separation $\varepsilon = (\phi - \phi_g)/\phi_g$ was used as an adjustable parameter quantifying the distance to the glass transition; the fitted values are also contained in Table II and the results are discussed in Sec. IV F.

References

Banchio, A. J., J. Bergenholtz, and G. Nägele, "Viscoelasticity and generalized Stokes-Einstein relations of colloidal dispersions," J. Chem. Phys. **111**, 8721–8740 (1999).

Callaghan, P., "Rheo-NMR and shear banding," Rheol. Acta **47**, 243–255 (2008).

Cheng, Z., J. Zhu, P. M. Chaikin, S.-E. Phan, and W. B. Russel, "Nature of the divergence in low shear viscosity of colloidal hard sphere dispersions," Phys. Rev. E **65**, 041405 (2002).

Crassous, J. J., M. Ballauff, M. Drechsler, J. Schmidt, and Y. Talmon, "Imaging the volume transition in thermosensitive core-shell particles by cryo-transmission electron microscopy," Langmuir **22**, 2403–2406 (2006b).

Crassous, J. J., R. Regisser, M. Ballauff, and W. Willenbacher, "Characterization of the viscoelastic behavior of complex fluids using the piezoelastic axial vibrator," J. Rheol. **49**, 851–863 (2005).

Crassous, J. J., M. Siebenbürger, M. Ballauff, M. Drechsler, D. Hajnal, M. Henrich, and M. Fuchs, "Shear stresses of colloidal dispersions at the glass transition in equilibrium and in flow," J. Chem. Phys. **128**, 204902 (2008a).

Crassous, J. J., M. Siebenbürger, M. Ballauff, M. Drechsler, O. Henrich, and M. Fuchs, "Thermosensitive core-shell particles as model systems for studying the flow behavior of concentrated colloidal dispersions," J. Chem. Phys. **125**, 204906 (2006a).

Crassous, J. J., A. Wittemann, M. Siebenbrger, M. Schrinner, M. Drechsler, and M. Ballauff, "Direct imaging of temperature-sensitive core-shell latexes by cryogenic transmission electron microscopy," Colloid Polym. Sci. **286**, 805–812 (2008b).

Deike, I., M. Ballauff, N. Willenbacher, and A. Weiss, "Rheology of thermosensitive latex particles including the high-frequency limit," J. Rheol. **45**, 709–720 (2001).

Dhont, J. and W. Briels, "Gradient and vorticity banding," Rheol. Acta **47**, 257–281 (2008).

Dingenouts, N., Ch. Norhausen, and M. Ballauff, "Observation of the volume transition in thermosensitive core-shell latex particles by small-angle x-ray scattering," Macromolecules **31**, 8912–8917 (1998).

Foss, D. R. and J. F. Brady, "Structure, diffusion and rheology of Brownian suspensions by Stokesian dynamics simulation," J. Fluid Mech. **407**, 167–200 (2000).

Fritz, G., W. Pechhold, N. Willenbacher, and J. W. Norman, "Characterizing complex fluids with high-frequency rheology using torsional resonators at multiple frequencies," J. Rheol. **47**, 303–319 (2003).

Fuchs, M. and M. Ballauff, "Flow curves of dense colloidal suspensions: Schematic model analysis of the shear-dependent viscosity near the colloidal glass transition," J. Chem. Phys. **122**, 094707 (2005).

Fuchs, M. and M. E. Cates, "Theory of nonlinear rheology and yielding of dense colloidal suspensions," Phys. Rev. Lett. **89**, 248304 (2002).

Fuchs, M. and M. E. Cates, "Schematic models for dynamic yielding of sheared colloidal glasses," Faraday Discuss. **123**, 267–286 (2003).

Fuchs, M. and M. E. Cates, "Mode-coupling approximations for Brownian particles in homogeneous steady shear flow," J. Rheol. (submitted) (2008).

Götze, W., "Some aspects of phase transitions described by the self consistent current relaxation theory," Z. Phys. B: Condens. Matter **56**, 139–154 (1984).

Götze, W., in *Liquids, Freezing and Glass Transition*, edited by J. P. Hansen, D. Levesque, and J. Zinn-Justin,

Session LI (1989) of Les Houches Summer Schools of Theoretical Physics, (North-Holland, Amsterdam, 1991).

Götze, W. and L. Sjögren, "Relaxation processes in supercooled liquids," Rep. Prog. Phys. **55**, 241–376 (1992).

Hajnal, D. and M. Fuchs, "Flow curves of colloidal dispersions close to the glass transition asymptotic scaling laws in a schematic model of mode coupling theory," Eur. Phys. J. E **28**, 125–139 (2009) .

Helgeson, M. E., N. J. Wagner, and D. Vlassopoulos, "Viscoelasticity and shear melting of colloidal star polymer glasses," J. Rheol. **51**, 297–316 (2007).

Heymann, L. and N. Aksel, "Transition pathways between solid and liquid state in suspensions," Phys. Rev. E **75**, 021505 (2007).

Horn, F. M., W. Richtering, J. Bergenholtz, N. Willenbacher, and N. J. Wagner, "Hydrodynamic and colloidal interactions in concentrated charge-stabilized polymer dispersions," J. Colloid Interface Sci. **225**, 166–178 (2000).

Isa, L., R. Besseling, and W. C. K. Poon, "Shear zones and wall slip in the capillary flow of concentrated colloidal suspensions," Phys. Rev. Lett. **98**, 198305 (2007).

Larson, R. G., *The Structure and Rheology of Complex Fluids* (Oxford University Press, New York, 1999).

Le Grand, A. and G. Petekidis, "Effects of particle softness on the rheology and yielding of colloidal glasses," Rheol. Acta **47**, 579–590 (2008).

Lionberger, R. A. and W. B. Russel, "High-frequency modulus of hard sphere colloids," J. Rheol. **38**, 1885–1908 (1994).

Manneville, S., "Recent experimental probes of shear banding," Rheol. Acta **47**, 301–308 (2008).

Meeker, S. P., W. C. K. Poon, and P. N. Pusey, "Concentration dependence of the low shear viscosity of suspensions of hard sphere colloids," Phys. Rev. E **55**, 5718–5722 (1997).

Olmsted, P. D., "Perspectives on shear banding in complex fluids," Rheol. Acta **47**, 283–300 (2008).

Petekidis, G., A. Moussaïd, and A. Pusey, "Rearrangements in hard sphere glasses under oscillatory shear strain," Phys. Rev. E **66**, 051402 (2002).

Pham, K. N., G. Petekidis, D. Vlassopoulos, S. U. Egelhaaf, W. C. K. Poon, and P. N. Pusey, "Yielding behavior of repulsion- and attraction-dominated colloidal glasses," J. Rheol. **52**, 649–676 (2008).

Phan, S.-E., M. Li, W. B. Russel, J. Zhu, P. M. Chaikin, and Ch. T. Lant, "Linear viscosity of hard sphere crystals from resonance detected with dynamic light scattering," Phys. Rev. E **60**, 1988–1998 (1999).

Purnomo, E. H., D. van den Ende, J. Mellema, and F. Mugele, "Linear viscoelastic properties of aging suspensions," Europhys. Lett. **76**, 74–80 (2006).

Purnomo, E. H., D. van den Ende, J. Mellema, and F. Mugele, "Rheological properties of aging thermosensitive suspensions," Phys. Rev. E **76**, 021404 (2007).

Russel, W. B., D. A. Saville, and W. R. Schowalter, *Colloidal Dispersions* (Cambridge University Press, New York, 1989).

Schaertl, W. and H. Sillescu, "Brownian dynamics of polydisperse colloidal hard spheres: Equilibrium structures and random close packings," J. Stat. Phys. **77**, 1007–1025 (1994).

Senff, H., W. Richtering, Ch. Norhausen, A. Weiss, and M. Ballauff, "Rheology of a temperature-sensitive core-shell latex," Langmuir **15**, 102–106 (1999).

Seth, Y. R., M. Cloitre, and R. T. Bonnecaze, "Elastic properties of soft particle pastes," J. Rheol. **50**, 353–376 (2006).

van Megen, W. and P. N. Pusey, "Dynamik light scattering study of the glass transition in a colloidal suspension," Phys. Rev. A **43**, 5429–5441 (1991).

van Megen, W. and S. M. Underwood, "Glass-transition in colloidal hard spheres—measurement and mode-coupling-theory analysis of the coherent intermediate scattering function," Phys. Rev. E **49**, 4206–4220 (1994).

Varnik, F. and O. Henrich, "Yield stress discontinuity in a simple glass," Phys. Rev. B **73**, 174209 (2006).